13th World Conference on Earthquake Engineering
Vancouver, B.C., Canada
August 1-6, 2004
Paper No. 3180

BEHAVIOR OF HIGH SEISMIC PERFORMANCE WALLS

Y. J. CHIOU[1], Y. L. MO[2], F. P. HSIAO[3], Y. W. LIOU[4], and M. S. SHEU[5]

SUMMARY

The structural behavior of high seismic performance walls subjected to reversed cyclic lateral loading were studied by testing large-scale framed shear wall specimens and numerical modeling. The cyclic constitutive relation of reinforced concrete and OpenSEES finite element code were adopted in numerical model. The walls were designed with 45° reinforcements. The numerical solutions agree well with the experimental results. The results show that the pinching effect, which frequently existed in the conventional shear walls, is remarkably improved in the new design high seismic performance walls. The larger steel ratio in the shear walls with 45° reinforcements induces less pinching effect. In addition, most of the maximum load, ultimate displacement, ductility factor, and energy absorption capacity of these new design framed shear walls are higher than the conventional ones. The new design shear wall possesses high potential to improve the seismic performance of buildings.

Keywords: concrete, elements, structural response, experimental testing, high seismic performance walls

INTRODUCTION

Framed shear walls are extensively used as the components of earthquake resistance buildings. However, the conventional shear walls, which the reinforcements are in vertical and horizontal directions, frequently possess pinching effect in the load-displacement curves. The pinching effect will reduce the energy dissipation capability of wall. The improvement of conventional shear wall to reduce the pinching effect sounds an essential research.

[1] Professor, Department of Civil Engineering, National Cheng Kung University, Tainan, Taiwan. E-mail: ceyjc@mail.ncku.edu.tw

[2] Professor, Department of Civil and Environmental Engineering, University of Houston, Houston, Texas, U.S.A. E-mail: yilungmo@egr.uh.edu

[3] Graduate student, Department of Civil Engineering, National Cheng Kung University, Tainan, Taiwan. E-mail: n6889117@dec4000.cc.ncku.edu.tw

[4] Professor, Department of Industrial Safety and Hygiene, Chia-Nan University of Pharmacy and Science, Tainan, Taiwan. E-mail: ywliou@mail.chna.edu.

[5] Professor, Department of Architecture, National Cheng Kung University, Tainan, Taiwan. E-mail: mssheu@mail.ncku.edu.tw

Benjamin and Williams [2] performed a series of tests on low-rise framed shear wall (Height/Width = 0.57) subjected to monotonic loading. They proposed a formula to predict the elastic-plastic load-displacement curves, and obtained the structural stiffness at various loads. Yamada et al. [13] tested a low-rise framed shear wall (Height/Width =0.44) by monotonic loading. They proposed a displacement model, and studied the parameters of wall thickness and steel ratio of wall. Barda et al. [1] presented tests on low-rise walls with boundary elements. They studied the parameters of vertical steel of boundary elements, horizontal and vertical steel of wall, and height to width ratio. Mau and Hsu [10] investigated the shear behavior of framed walls and proposed a formula to predict the strength of walls. Mo and Kuo [11] presented a displacement control test on small-scale framed shear wall subjected to reversed cyclic lateral loading. They studied the parameters of structural dimension and concrete strength. The experimental results were compared with solutions obtained by truss model and IDARC software, and a large deviation was found between test and analytical results. These aforementioned shear walls are conventional walls. Recently, Mansour and Hsu [9] presented the experimental results of reinforced concrete elements under cyclic shear. They found that when the reinforcements are parallel to the principal directions of the element, there is almost no pinching effect in the load-displacement curves. These experimental results show that the orientation of reinforcements will affect the structural behavior of wall elements.

This study investigates the structural behavior of high seismic performance walls subjected to reversed cyclic lateral loading by testing large-scale framed shear wall specimens and numerical modeling. The cyclic constitutive relation of reinforced concrete [8] and OpenSEES finite element code [4] were adopted in numerical model. The walls were designed with 45° reinforcements. Four large-scale specimens, including mid-, and low-rise high seismic performance framed shear walls were presented. The experimental results were compared with those of four corresponding conventional specimens worked by the authors previously [3].

EXPERIMENTAL PROGRAM

Experimental Setup

Fig. 1 shows the schematic configuration of the test setup. Each specimen was bolted at the steel foundation, which was then connected to the strong floor. A manually operated hydraulic jack with a loading capacity of $\pm$1500kN and a stroke of $\pm$200mm supplied the lateral force. A reversed cyclic loading history was adopted, as shown in Fig. 2. The experiment was first load-controlled when the applied lateral force was smaller than the yield load or three times of the crack load. Afterwards, the experiment was transformed to displacement-control. The lateral displacements were measured by linear variable differential transformers (LVDT) and the force was measured by load cell. The measured force and displacement were collected by TDS-302 data logger. The experiment was monitored by the load-displacement curve.

Design of Specimens

Fig. 3 shows a primary stress analysis of mid- and low-rise homogeneous elements subjected to horizontal force. A rightward horizontal force is applied at the upper right corner of the element. It is found that the principal directions are not fixed. The angles of principal directions change smoothly from left side to right side. Around the central region, the principal directions are 34.1° to 55.9° for mid-rise element, and 38.7° to 51.3° for low-rise element. Referring to Figs. 3a and 3b, there are nearly parallel patterns of principal directions for both mid-rise and low-rise elements. Most of the principal directions in the central region are approximately 45°. At the first attempt, the high seismic performance walls are designed by adopting 45° reinforcements in this study.

Four high seismic performance specimens including mid-, and low-rise shear walls subjected to reversed cyclic lateral loading were presented. These specimens were two mid-rise framed walls with 45° reinforcements (MWFD1, MWFD2), two low-rise framed walls with 45° reinforcements (LWFD1, LWFD2). The dimensions of all columns and beams were 250mm × 250mm and 300mm × 400mm, respectively. The #5 steel bars (diameter of 16 mm) were adopted for both beam and columns. The height and width of mid-rise shear walls were 2000mm. The height and width of low-rise shear walls were 2000mm and 2700mm, respectively. The wall thickness of all specimens was 120mm. Table 1 summarizes the properties of all specimens. The reinforcement layout of representative specimens are presented in Fig. 4.

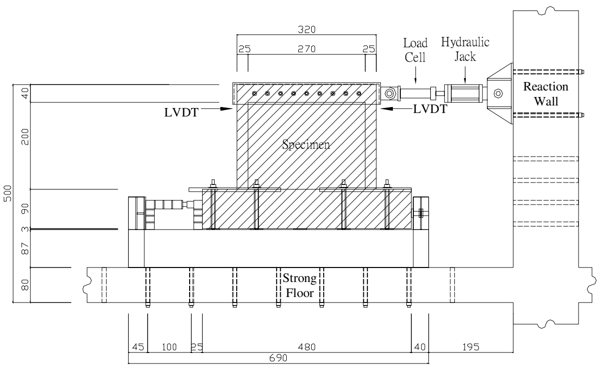

Fig. 1 Schematic configuration of experimental setup

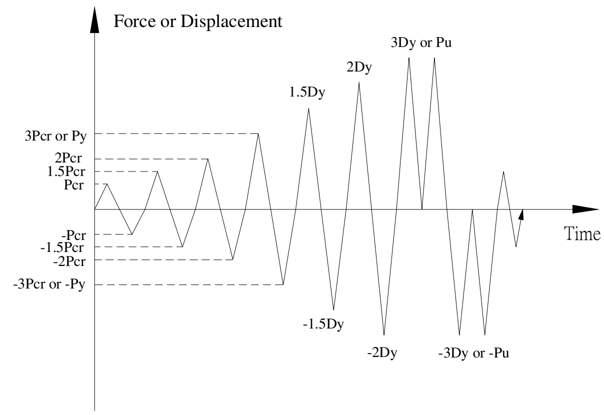

Fig. 2 Loading history

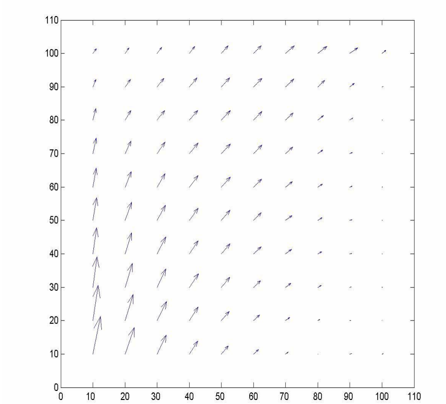

(a) Principal direction of mid-rise element

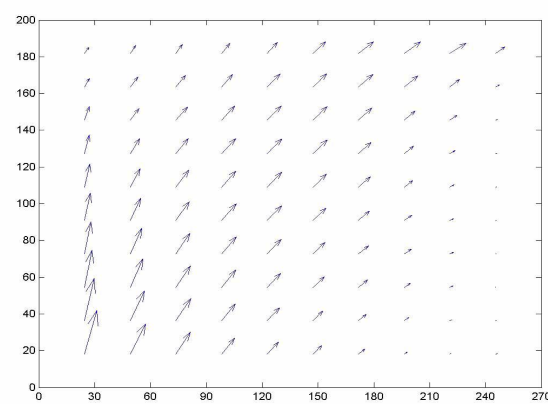

（b）Principal direction of low-rise element

Fig. 3 Fundamental analysis of principal direction

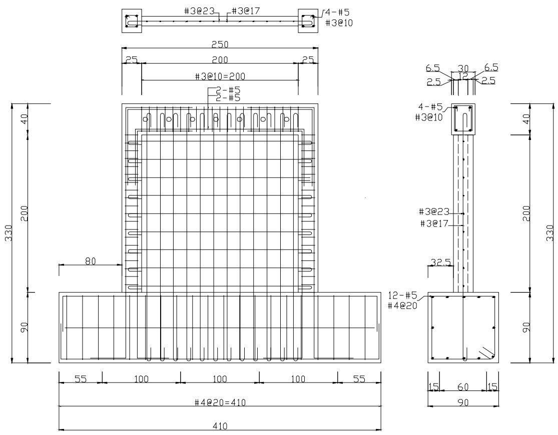

（a）**Specimen MWF1 [3]**

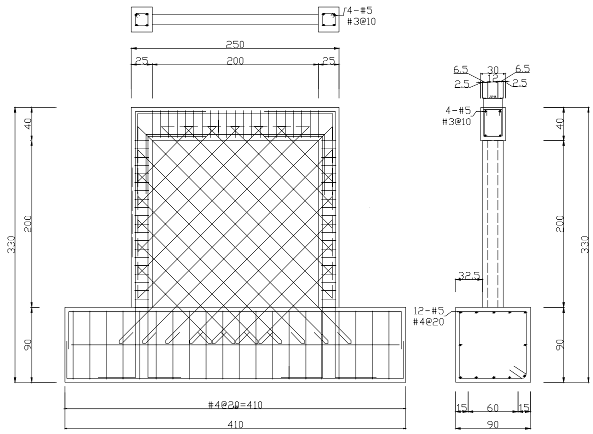

（b）**Specimen MWFD1**

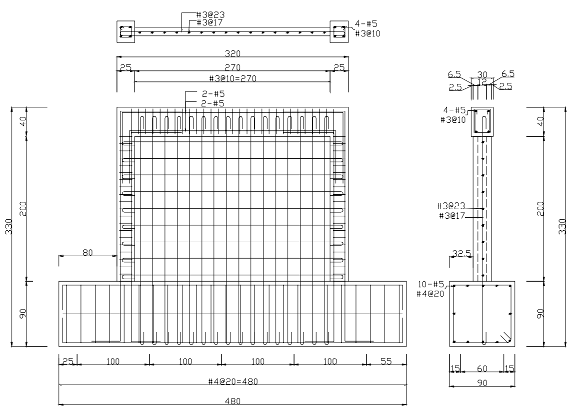

（c）**Specimen LWF1 [3]**

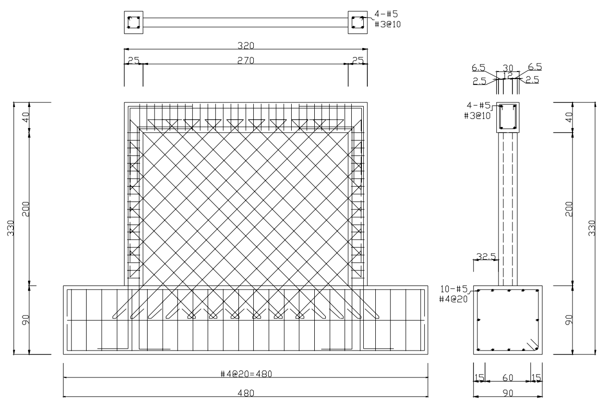

（d）**Specimen LWFD1**

Fig.4 Reinforcement layout of representative specimens

Table 1 Specimen cross-section and reinforcement properties

Specimen	Dimension of specimen		Dimension of wall [a]		Column (mm×mm)	ρ_c	Vertical steel Bars (mm)	Horizontal steel Bars (mm)
	H (mm)	W (mm)	H_w (mm)	W_w (mm)				
MWF1[3]	2400	2500	2000	2000	250×250	4-D16	#3@170	#3@230
MWFD1	2400	2500	2000	2000	250×250	4-D16	13-D10, spacing 200mm, with 45°	
MWF2[3]	2400	2500	2000	2000	250×250	4-D16	#3@230	#3@230
MWFD2	2400	2500	2000	2000	250×250	4-D16	11-D10, spacing 218mm, with 45°	
LWF1[3]	2400	3200	2000	2700	250×250	4-D16	#3@170	#3@230
LWFD1	2400	3200	2000	2700	250×250	4-D16	16-D10, spacing 204mm, with 45°	
LWF2[3]	2400	3200	2000	2700	250×250	4-D16	#3@230	#3@230
LWFD2	2400	3200	2000	2700	250×250	4-D16	14-D10, spacing 258mm, with 45°	

[a] Thickness of all walls is 120 mm.

NUMERICAL ANALYSIS

Constitutive Relation of Reinforced Concrete Element

Referring to Fig. 5, the modified Kent & Park model for stress-strain curves of concrete confined by rectangular hoops [12] is adopted for beam-column element. The loading and unloading path is followed the model of Karsan and Jirsa [7]. A bi-linear constitutive relation (Fig. 6) is chosen for the reinforcement of beam-column element.

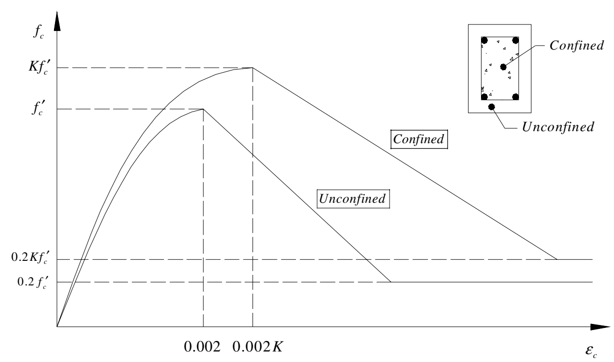

Fig. 5 Modified Kent & Park model for stress-strain curves of concrete confined by rectangular hoops

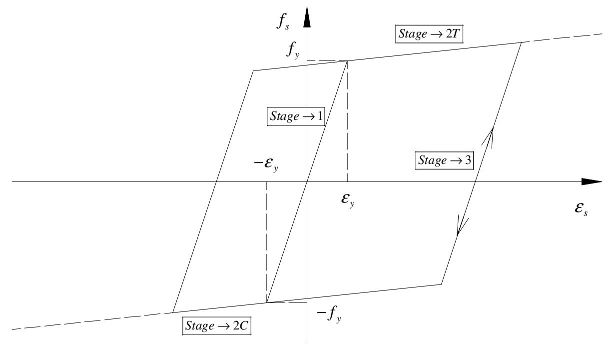

Fig. 6 Bi-linear stress-strain curves for steel with reversed loading

A cyclic stress-strain curves of concrete and steel bars (Figs. 7 and 8) proposed by Mansour and Hsu [8] is used to model the shear wall. Referring to Fig. 8, the prototype cyclic stress-strain curves of embedded steel bars is represented by Ramber-Osgood model. A linear approximation is proposed in this study. The modified equations are as follows.

Stage 1

$$f_s = E_s \varepsilon_s \qquad (-\varepsilon_n \le \varepsilon_s \le \varepsilon_n) \qquad (1)$$

where $\varepsilon_n = \varepsilon_y (0.93 - 2B)$ is the initial yield strain of embedded steel , ε_y is the initial yield strain of steel, $B = \frac{1}{\rho}\left(\frac{f_{cr}}{f_y}\right)^{1.5}$, f_y is the initial yield stress of steel, $f_{cr} = 0.31\sqrt{f_c'(MPa)}$ is the crack stress of concrete, $f_c^{'}$ is the compressive strength of concrete, and $\rho \ge 0.25\%$.

Stage 2T

$$f_s = f_y \left[(0.91 - 2B) + \left(0.02 + 0.25B \frac{\varepsilon_s}{\varepsilon_y} \right) \right] \qquad (\varepsilon_s > \varepsilon_n) \qquad (2)$$

Stage 2C

$$f_s = -f_y \left[(0.91 - 2B) + \left(0.02 + 0.25B \frac{\varepsilon_s}{\varepsilon_y} \right) \right] \qquad (\varepsilon_s < -\varepsilon_n) \qquad (3)$$

Stage 3

Three linear lines approximate the Ramber-Osgood curve. The intersection stresses are $f_{m1}=0$ and $f_{m2}=-0.65f_y$. The intersection strains ε_{m1} and ε_{m2} are

$$\varepsilon_{m1}=\varepsilon_i-\frac{f_i}{E_s}\left[1+A^{-R}\left|\frac{-f_i}{f_y}\right|^{R-1}\right] \tag{4}$$

$$\varepsilon_{m2}=\varepsilon_i-\frac{0.65f_y+f_i}{E_s}\left[1+A^{-R}\left|\frac{-0.65f_y-f_i}{f_y}\right|^{R-1}\right] \tag{5}$$

where f_i and ε_i are stress and strain of steel at load reversal point, $R=10k_p^{-0.2}$, $A=1.9k_p^{-0.1}$, $k_p=\dfrac{\varepsilon_p}{\varepsilon_n}=\dfrac{\varepsilon_i-\varepsilon_n}{\varepsilon_n}$, ε_p is the plastic strain of steel, and ε_n is the initial yield strain of embedded steel.

Stage 4

Similar to Stage 3, three linear lines approximate the Ramber-Osgood curve. However, the intersection stresses are $f'_{m1}=0$ and $f'_{m2}=0.65f_y$. The intersection strains ε'_{m1} and ε'_{m2} are

$$\varepsilon'_{m1}=\varepsilon_i-\frac{f_i}{E_s}\left[1+A^{-R}\left|\frac{-f_i}{f_y}\right|^{R-1}\right] \tag{6}$$

$$\varepsilon'_{m2}=\varepsilon_i+\frac{0.65f_y-f_i}{E_s}\left[1+A^{-R}\left|\frac{0.65f_y-f_i}{f_y}\right|^{R-1}\right] \tag{7}$$

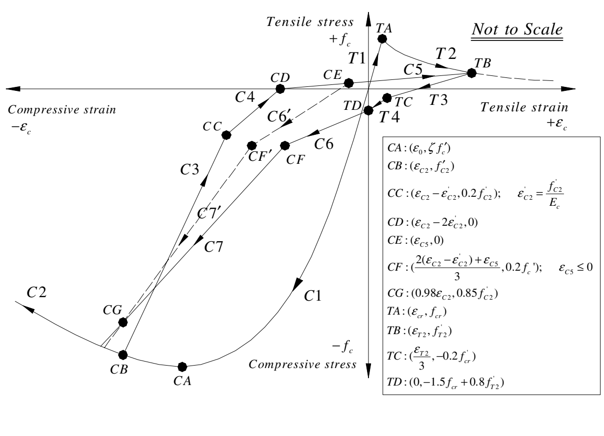

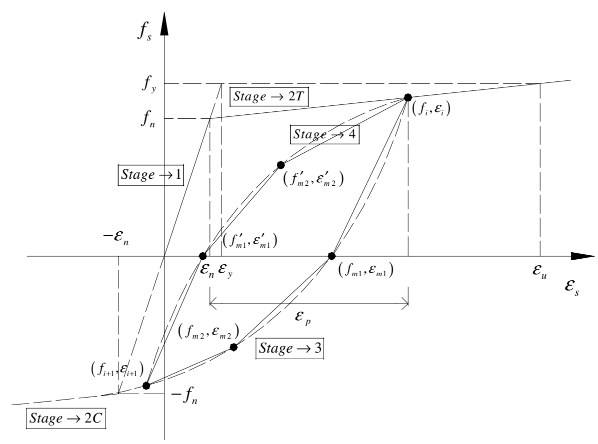

Fig. 7 Mansour and Hsu model for cyclic smeared stress-strain curves of concrete

Fig. 8 Mansour and Hsu model for cyclic smeared stress-strain curves of mild steel bars embedded in concrete

Element Stiffness of Reinforced Concrete Shear Wall

Referring to Fig. 9, the crack direction of a concrete element is assumed to coincide with the principal direction. The material stiffness matrix of a plane concrete element (Hsu and Zhu [6]) is

$$[E_c]' = \begin{bmatrix} \dfrac{\overline{E}_{c1}}{1-\nu_{12}\nu_{21}} & \dfrac{\nu_{12}\overline{E}_{c1}}{1-\nu_{12}\nu_{21}} & 0 \\ \dfrac{\nu_{21}\overline{E}_{c2}}{1-\nu_{12}\nu_{21}} & \dfrac{\overline{E}_{c2}}{1-\nu_{12}\nu_{21}} & 0 \\ 0 & 0 & G_c \end{bmatrix} \tag{8}$$

where $\overline{E}_{c1}$ and $\overline{E}_{c2}$ are tangent moduli, G_c is shear modulus,

$$G_c = \frac{\sigma_{c1} - \sigma_{c2}}{2(\varepsilon_{c1} - \varepsilon_{c2})} \tag{9}$$

σ_{c1} and σ_{c2} are average stress, ε_{c1} and ε_{c2} are average strain, ν_{12} and ν_{21} are Hsu/Zhu ratio,

$$\nu_{12} = 0.2 + 850\varepsilon_{sf} \qquad (\varepsilon_{sf} \le \varepsilon_y) \tag{10}$$

$$\nu_{12} = 1.9 \qquad (\varepsilon_{sf} > \varepsilon_y) \tag{11}$$

ε_{sf} is average tensile stress of yielded steel, ν_{21} is chosen to be 0 in this study. The material stiffness matrix of reinforcement is

$$[E_s]'_i = \begin{bmatrix} \rho_i \cdot \overline{E}_{si} & 0 & 0 \\ 0 & 0 & 0 \\ 0 & 0 & 0 \end{bmatrix} \tag{12}$$

where ρ_i is reinforcement ratio, and $\overline{E}_{si}$ is tangent modulus. The material stiffness for concrete and reinforcement components in the global reference system are written as

$$[E_c] = [T_c]^T [E_c]' [T_c] \tag{13}$$

$$[E_s]_i = [T_s]_i^T [E_s]'_i [T_s]_i \tag{14}$$

where [T] is transformation matrix,

$$[T] = \begin{bmatrix} \cos^2\psi & \sin^2\psi & \sin\psi\cos\psi \\ \sin^2\psi & \cos^2\psi & -\cos\psi\sin\psi \\ -2\cos\psi\sin\psi & 2\cos\psi\sin\psi & \left(\cos^2\psi - \sin^2\psi\right) \end{bmatrix} \tag{15}$$

$\psi = \phi + \beta = \pi - \theta_c + \beta$ for concrete component, and $\psi = \alpha_i + \beta$ for reinforcement component. The total material stiffness matrix for reinforced concrete element is evaluated as

$$[E] = [E_c] + \sum_{i=1}^{2} [E_s]_i \tag{16}$$

The element stiffness matrix can be derived as

$$[k] = \int [B_e]^T [E][B_e] dV \tag{17}$$

where $\left[B_e\right]$ is shape function matrix.

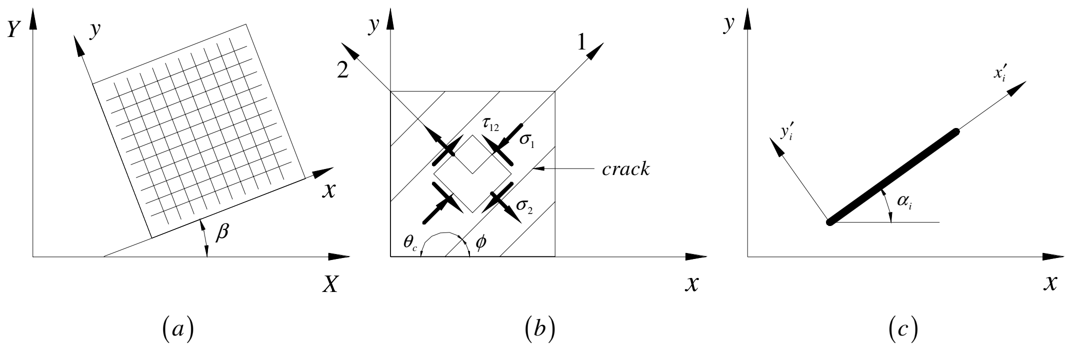

Fig. 9 Coordinates systems for reinforced concrete element: (a) global system of reinforced concrete element; (b) local system of concrete component; and (c) local system of reinforcement component

Implementation of Nonlinear Analysis

The object orient program OpenSEES finite element code [4] is adopted in this study. The aforementioned cyclic constitutive relation of reinforced concrete element is developed to be a module of OpenSEES. Referring to Fig. 10, the columns are modeled to be nonlinear beam-column elements, the beam is assumed to be rigid, and the shear wall is modeled by four-node isoparametric elements. The wall is divided into 25 elements, and each column is represented by 5 elements. The nonlinear analysis is implemented by displacement control and incremental analysis.

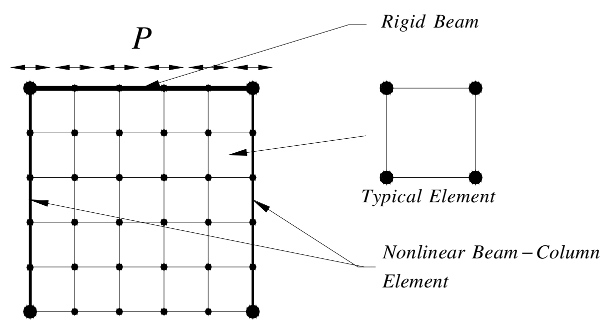

Fig. 10 Finite element mesh of reinforced concrete framed-shear wall specimen

RESULTS AND DISCUSSION

Table 2 summarizes the experimental results. The energy absorption is defined to be the area bounded by the envelope of positive load-displacement curve. The ultimate displacement Δ_u is defined to be the displacement corresponding the load descended steeply. This definition is different from the previous study [3], which Δ_u is defined to be the displacement corresponding to the maximum load.

The crack patterns and load-displacement curves of tested specimens are shown in Figs. 12 and 13, respectively. Fig. 13 shows that the numerical solutions agree well with the experimental results. The proposed numerical model is demonstrated to be capable of analyzing cyclic structural behavior of framed shear wall.

Table 2 Summary of experimental results

Specimen	f'_c (MPa)	f_y Steel in column (MPa)	f_y Steel in wall (MPa)	P_{cr} (kN)	Δ_{cr} (mm)	P_y (kN)	Δ_y (mm)	P_u (kN)	Δ_u (mm)	Ductility factor (Δ_u / Δ_y)	Energy absorption (kN-mm)
MWF1	23.45	390.00	458.72	214.84	0.70	460.09	5.60	537.59	42.97	7.67	20942
MWFD1	20.77	372.14	428.38	236.18	0.68	424.34	5.32	541.94	40.07	7.53	20550
MWF2	23.45	390.00	458.72	155.98	0.42	453.22	7.33	515.03	58.84	8.03	26409
MWFD2	20.77	372.14	428.38	138.18	0.014	412.58	5.09	518.42	35.27	6.93	22985
LWF1	23.75	390.00	458.72	308.03	0.61	658.25	7.09	808.34	30.32	4.28	21863
LWFD1	19.89	372.14	428.38	235.2	0.38	686.98	5.92	840.84	48.37	8.17	31976
LWF2	23.75	390.00	458.72	222.69	0.33	593.51	5.15	736.73	24.14	4.69	15071
LWFD2	19.89	372.14	428.38	233.24	0.48	643.86	5.04	754.60	35.27	7.00	23189

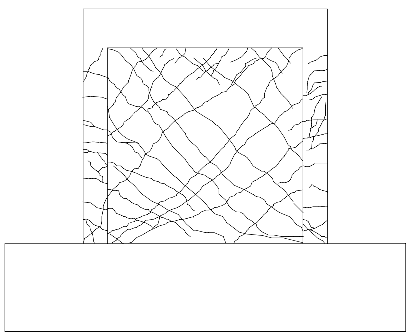

（a）Specimen MWF1[3]

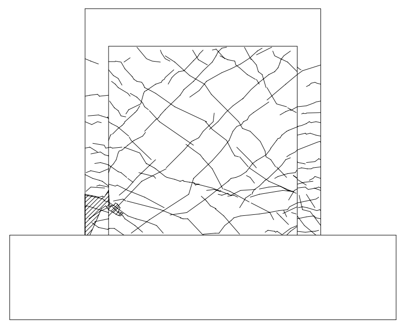

（b）Specimen MWFD1

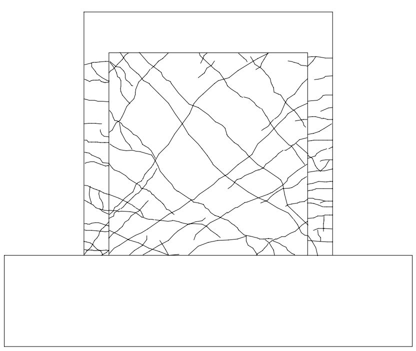

（c）Specimen MWF2 [3]

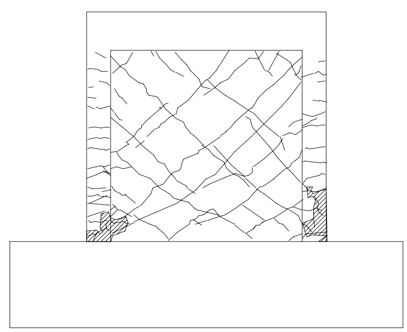

（d）Specimen MWFD2

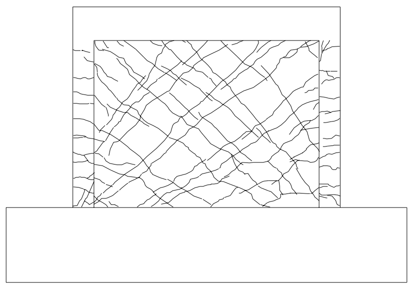

（e）Specimen LWF1 [3]

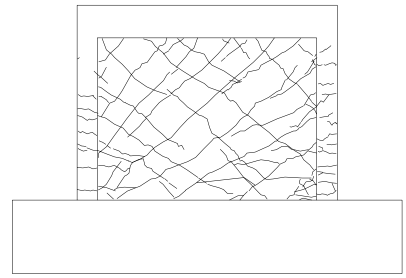

（f）Specimen LWFD1

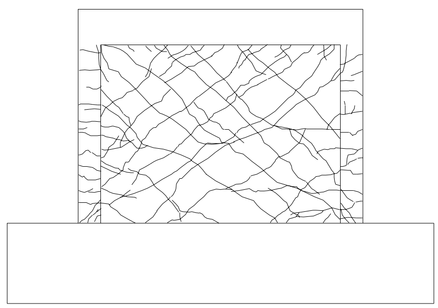

（g）Specimen LWF2 [3]

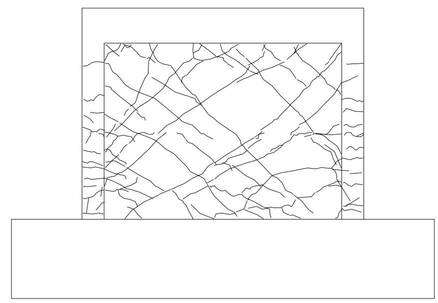

（h）Specimen LWFD2

Fig.12 Crack patterns of tested specimens

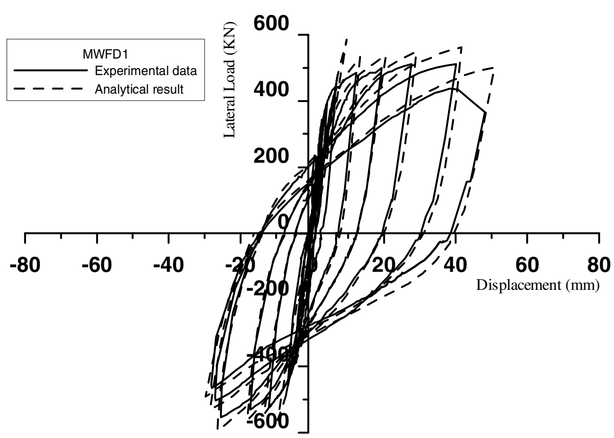

（a）Specimen MWFD1

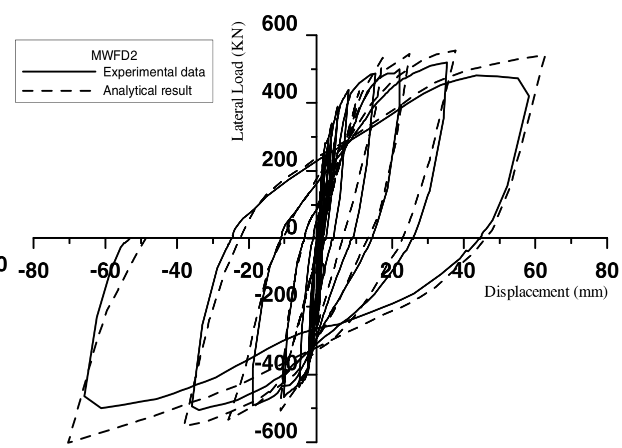

（b）Specimen MWFD2

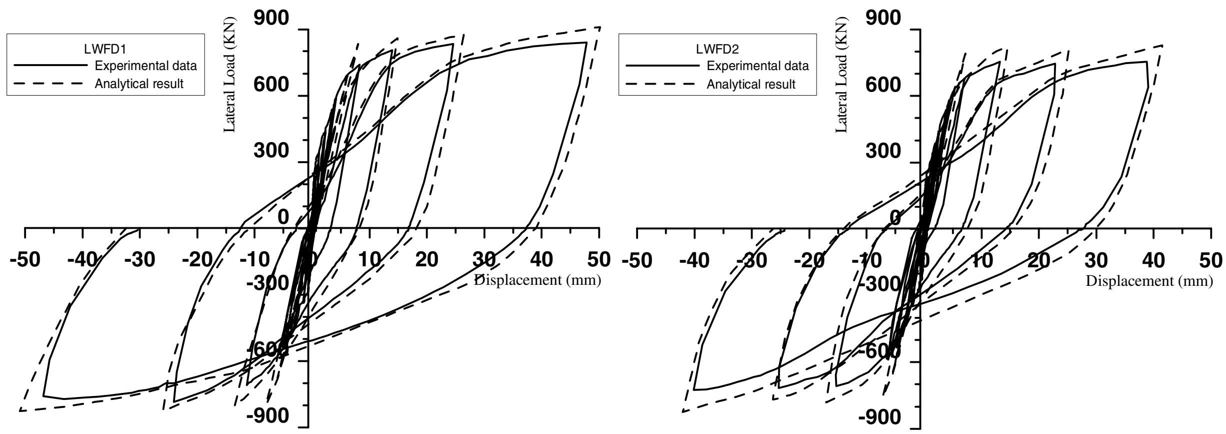

（c）**Specimen LWFD1** （d）**Specimen LWFD2**

Fig.13 Comparison of numerical results with experimental load-displacement curves

Referring to Fig. 12, the crack patterns of all high seismic performance specimens show no significant difference with the corresponding conventional specimens. However, Table 2 shows that most of the maximum load P_u, ultimate displacement Δ_u, ductility factor, and energy absorption of high seismic performance specimens are found to be larger than those of the corresponding conventional specimens.

The ultimate displacement, ductility factor, and energy absorption of two mid-rise framed walls with 45° reinforcements (MWFD1, MWFD2) are smaller than the corresponding conventional specimens (MWF1, MWF2). However, referring to Figs. 13a and 13b, the pinching effect is remarkably improved. During test, both MWFD1 and MWFD2 were flexural failure and crushed at the bottom of boundary columns (Figs. 12b, 12d). It was justified that because the vertical components of 45° reinforcements are less than the conventional ones, the flexural resistance of MWFD1 and MWFD2 are insufficient.

The maximum load, ultimate displacement, ductility factor, and energy absorption of two low-rise framed walls with 45° reinforcements (LWFD1, LWFD2) are larger than the corresponding conventional specimens (LWF1, LWF2). Referring to Figs. 13c and 13d, the pinching effect is remarkably improved. Because these two specimens were adopted as subsequently repaired experiment specimens, they were not tested to complete failure. There is no load descended steeply in the load-displacement curve (Figs. 13c, 13d). The current ultimate displacement, ductility factor, and energy absorption are supposed to be lower than the expected exact ones.

CONCLUSIONS

This study presents the experimental and numerical analysis on structural behavior of high seismic performance walls subjected to reversed cyclic lateral loading. Based on the primary analysis of principal direction, the reinforcements of wall were designed with 45° reinforcements. Four large-scale specimens, including mid-, and low-rise framed shear walls were presented. The experimental results were compared with those of four corresponding conventional specimens worked by the authors previously [3].

The numerical solutions agree well with the experimental results. The proposed numerical model is demonstrated to be capable of analyzing cyclic structural behavior of framed shear wall. The results show that the pinching effect, which frequently existed in the conventional shear walls, is remarkably improved in the new design ones. The new design shear walls possess more percentage of ductile structural behavior. The larger steel ratio in the shear walls with 45° reinforcements induces less pinching effect. In addition, most of the maximum load, ultimate displacement, ductility factor, and energy absorption capacity of these new design framed shear walls are higher than the conventional ones. The new design shear walls possess high potential to improve the seismic performance of buildings.

ACKNOWLEDGEMENTS

This study was supported by the National Science Council, Taiwan under grants NSC 91-2211-E-006-078, and NSC 92-2625-Z-006-010.

REFERENCES

1. Barda, F., J. M. Hanson, and W. G. Corley, *Shear Strength of Low-Rise Walls with Boundary Elements*, Porland Cement Association publication RD043D, 1976.
2. Benjamin, J. R., and H. A. Williams, “The Behavior of One-Story Reinforced Shear Wall,” *Journal of the Structural Division, ASCE*, 1957; May, 1254: 1-49.
3. Chiou, Y. J., Y. L. Mo, F. P. Hsiao, Y. W. Liou, and M. S. Sheu, “Experimental and Analytical Studies on Large-Scale Reinforced Concrete Framed Shear Walls,” ACI SP-211, *Large-Scale Structural Testing*, American Concrete Institute, 2003: 201-221.
4. Fenves, G. L., F. McKenna, and M. H. Scott, *OpenSees User and Developer Workshop*, Workshop Handout, Pacific Earthquake Engineering Research Developer Center, University of California, Berkeley, U.S.A. 2001.
5. Fintel, M., “Shear wall—An Answer for Seismic Resistance,” *Concrete International*, 1991; July: 48-53, .
6. Hsu, T. T. C. and R. R. H. Zhu, “Softened Membrane Model for Reinforced Concrete Elements in Shear,” *Structural Journal of the American Concrete Institute*, 2002; 99(4): 460-469.
7. Karsan, I. D. and J. O. Jirsa, “Behavior of Concrete under Compressive Loadings,” *Journal of the Structural Division*, *ASCE*, 1969; 95(ST12): 2543-2563.
8. Mansour, M., J. Y. Lee, and T. T. C. Hsu, “Cyclic Stress-Strain Curves of Concrete and Steel Bars in Membrane Elements,” *Journal of the Structural Division*, *ASCE*, 2001; 127, (12): 1402-1411.
9. Mansour, M. and Hsu, T. T. C., "Behavior of Reinforced Concrete Elements Under Cyclic Shear: Part I - Experiments," *Journal of Structural Engineering, ASCE*, (accepted for publication in 2003).
10. Mau, S. T. and T. T. C. Hsu, “Shear Behavior of Reinforced Concrete Framed Wall Panels with Vertical Load,” *ACI Structural Journal*, 1987; 84(2): 228-234.
11. Mo, Y. L. and C. J. Kuo, “Structural Behavior of Reinforced Concrete Frame-Wall Components,” *Materials and Structures*, 1998; 31: 609-615.
12. Sheikh, S. A. and S. M. Uzumeri, “Analytical Model for Concrete Confinement in Tied Columns,” *Journal of the Structural Division*, *ASCE*, 1982; 108(12): 2703-2722.
13. Yamada, M., H. Kawamura, and K. Katagihara, “Reinforced Concrete Shear Walls without Openings, Test and Analysis,” ACI SP-42, *Shear in Reinforced Concrete*, Vols. 1 & 2, American Concrete Institute, 1974: 539-558.